We are IntechOpen,
the world's leading publisher of
Open Access books
Built by scientists, for scientists

4,800

Open access books available

122,000

International authors and editors

135M

Downloads

Our authors are among the

154

Countries delivered to

TOP 1%

most cited scientists

12.2%

Contributors from top 500 universities

CLARIVATE ANALYTICS

BOOK CITATION INDEX

INDEXED

WEB OF SCIENCE™

Selection of our books indexed in the Book Citation Index
in Web of Science™ Core Collection (BKCI)

Interested in publishing with us?
Contact book.department@intechopen.com

Numbers displayed above are based on latest data collected.
For more information visit www.intechopen.com

Nanomechanics of Amyloid Materials Studied by Atomic Force Microscopy

Guanghong Zeng, Yusheng Duan,
Flemming Besenbacher and Mingdong Dong
Interdisciplinary Nanoscience Center (iNANO), Aarhus University
Denmark

1. Introduction

1.1 Amyloid materials and their mechanical properties

Amyloids are usually used to refer to a wide range of fibrous nanostructures formed from natural and synthetic proteins and peptides. The self-propagating protein aggregates are rich in β-sheets, which stack in hundreds to thousands units perpendicular to the fibrous axis, forming fibrils 5-15 nm in width and several micrometers in length (Dobson, 1999; Jaroniec et al., 2004; Luhrs et al., 2005; Sawaya et al., 2007; Wasmer et al., 2008). The structural trait gives amyloids the so called "cross-β" diffraction pattern under X-ray crystallography as well as some tinctorial properties which they share in common, such as Congo red and thioflavin-T binding ability (Westermark et al., 1999) and the characteristic apple-green birefringence under polarized light when stained with Congo red.

While the study of amyloids was initiated a long time ago, the interest in exploring their structures and understanding the structural basis of their formation has been mainly stimulated by their association with neurodegenerative disorders such as Alzheimer's, and Parkinson's diseases (Selkoe, 2001; Tan & Pepys, 1994). Amyloidosis, the process in which soluble protein are deposited pathologically to form amyloid plaques, is believed to be the central step which initiates a series of events which eventually lead to neuron degeneration (Bucciantini et al., 2002; Paravastu et al., 2008). As more diseases such as type II diabetes, Creutzfeldt-Jakob disease (CJD or "Mad Cow" disease), and rheumatoid arthritis are found to be related to amyloidosis (Chiti & Dobson, 2006), amyloids have gained notorious reputation for a long time. However, during the past 10 years, it has been found that many living organisms take advantage of specific proteins' ability to form fibrous amyloids to perform their ordinary functions (Fowler et al., 2007). Bacteria form an extracellular amyloid matrix for their surface adhesion and colony formation (Chapman et al., 2002); in mammal cells, amyloids facilitate and regulate the synthesis of melanin (Fowler et al., 2005); they also serves as a regulatory motif in human hemostasis (Shibayama et al., 1999). These discoveries make amyloids very interesting because of their dual identities as pathogenic factors and functional components.

From the aspect of nanoengineering, amyloids are unique materials because of their highly ordered structure. The cooperative hydrogen-bonds between the well-stacked β-sheets

allows amyloid fibrils to grow into microns in length, reaching maximum strength in supermolecular assemblies (Fowler, et al., 2005) that can hardly be achieved by artificial materials. Similar structures are found in silk, one of the natural materials with the highest strength. With their unique well-ordered fibrous structure, amyloid fibrils have found applications in template synthesis for metal nanowires (Carny et al., 2006; Reches & Gazit, 2003; Scheibel et al., 2003), solar cells (Barrau et al., 2008; Channon et al., 2009; Liang et al., 2008), tissue engineering (Ellis-Behnke et al., 2006; Holmes et al., 2000), and drug delivery (Maji et al., 2008).

Understanding the mechanical properties are crucial to biological materials, as the mechanical information reveals their structural origin as well as how the materials contribute to the biological system by interacting with other components. This is especially challenging for amyloids, not only because of their micrometer length and nanometer width which makes them inaccessible for traditional mechanical tests, but also because they have hierarchical structures. Several thin fibrils, or protofilaments, are assembled in a twisted way to form an amyloid fibril. To make it even worse, more and more evidence suggests that amyloids are structurally diverse (Toyama & Weissman, 2011). Therefore it is necessary to measure the mechanical properties at a single fibril level, which falls in the range of nanometers.

1.2 AFM as a unique tool for nanomechanics of amyloid materials

Because the width of the amyloid fibril is usually several nanometers, we have to turn to single-molecular force techniques to explore their nanomechanics. Although new techniques are emerging constantly, the most commonly used ones for single-molecule manipulation and force spectroscopy are atomic force microscopy (AFM), optical tweezers, and magnetic tweezers (Neuman & Nagy, 2008). Optical tweezers and magnetic tweezers share a common mechanism, where objects are trapped either in an optical field (Ashkin et al., 1986) or in a magnetic field (Strick et al., 2000). In both methods, the interaction forces are determined by displacement from the trapped location when no external forces are present. The stiffness of the trapping is linearly determined by the strength of optical trapping or magnetic field, which is tuned by the setup of the laser system or magnets. Thus both methods are able to detect very low force, down to 10^{-1} pN for optical tweezers and 10^{-3} pN for magnetic tweezers. However, the upper limit of the detection is determined by the strength of the trapping force as well as the linear range, which is up to 100 pN for both methods (Neuman & Nagy, 2008). Unfortunately, in many cases of nanomechanical measurement beyond the molecular level, the forces go right out of this limit.

Atomic force microscopy (AFM) (Binnig et al., 1986), operating with a completely different mechanism, is a solution to these cases. Among the three techniques discussed, AFM is perhaps the most popular one. AFM works with a simple mechanism (Figure 1). Basically, it works with a force probe, which is a microfabricated cantilever with a sharp tip mounted on one end. As a piezo system controls the scanning of the tip on the sample surface in the horizontal (x and y) and vertical (z) direction, the deflection of the cantilever as a result of the interactions between the tip and sample is translated by a laser beam reflected on the back of the cantilever. Displacement of the laser beam on the photodiode is recorded as an amplified signal of the cantilever deflection. AFM allows the mapping of the surface down to sub-nanometer range, and works on all types of surfaces, regardless of whether they are
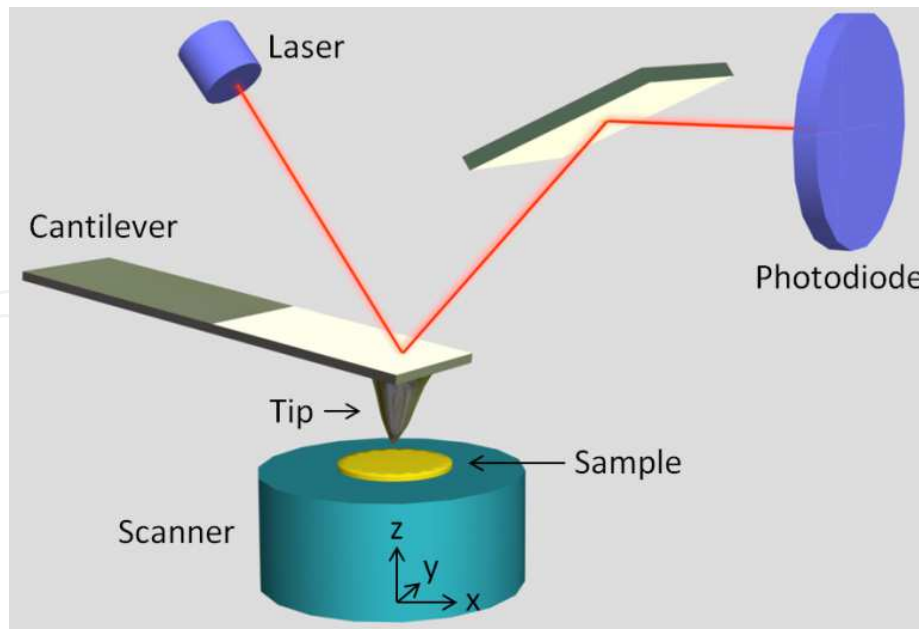
Fig. 1. Schematic illustration of the principles of AFM. The scanner is composed of three piezo components, which control the horizontal (x and y) and vertical (z) movement of the sample.

conductive or not. Another major advantage is that AFM works in liquid environment, which makes it superior to other imaging techniques for the measurement of biological samples under physiological conditions. Besides, sample preparation is simple and fast, compared to other imaging techniques such as electron microscopy.

Although AFM was initially developed for imaging, it is also a powerful tool for the measurement of forces with piconewton resolution. In the force spectroscopy mode (Weisenhorn et al., 1989), instead of scanning across the sample surface, the AFM probe moves vertically at a specified point on the sample, recording a deflection-displacement curve, which is subsequently converted to a force-extension curve by suitable calibrations. Within the operation range, the cantilever behaves as a linear spring. Therefore, the force detected by AFM is determined by the spring constant of the cantilevers used. Due to the large size and relatively high stiffness of the cantilevers, AFM operates at a much higher force range compared to that of the optical and magnetic tweezers, typically from 10 pN to 10^4 pN. The broad detection range is enabled by the extensive choices of cantilevers for a specific measurement.

Another advantage for AFM is the combination of high resolution imaging and force spectroscopy, which makes it possible to locate the region of interest in nanometer precision, especially when the objects have heterogeneous features, such as the case in amyloid materials. Also, it is a major advantage for AFM to operate at physiological conditions, which allows the investigation of amyloid fibrils under conditions similar to their native environment. For these reasons, although AFM is a new tool for amyloid research with the first paper published in 1995 (Oda et al., 1995), it has become a major tool for the characterization of amyloid materials, providing complementary and unique possibilities for amyloid research compared to the electron microscopy, which had been the major imaging tool for bio-samples such as amyloid materials before AFM was invented.

In this chapter, we will focus on the study of mechanical properties of amyloid materials with AFM. By introducing AFM based nanoindentation and force spectroscopy, we are going to illustrate how AFM as a nanotool reveals information on the stiffness, elastic properties, and rupture strength of amyloid materials, as well as their interactions with each other and the environment. Limitations and future directions will also be discussed, considering that AFM is a fast evolving technique, with a lot of major progresses made in the recent years.

2. AFM based nanoindentation

2.1 General principle

In a typical nanoindentation measurement, it usually starts with a topography image. The tip is then maneuvered to a point of interest, and brought into contact with the sample by vertical movement. After the contact, the tip and sample are pushed further towards each other, until a predefined force is reached. At this point the tip is retracted. During this approach-retract cycle, the cantilever deflection is continuously recorded, and force-distance curves are obtained after cantilever deflection is transformed into force by cantilever calibration. The curves are then fitted with suitable model to give the mechanical properties of the sample.

During the force experiment, the instrument records the deflection of the cantilever (d) (which is defined by the change of reflection angle (θ) of the laser beam) versus the displacement of the z piezo (Z). In order to convert the deflection vs. displacement curve to force vs. indentation curve, which is a premise for the fitting of the results, several treatment and calibration steps have to be taken. First, the indentation δ is calculated by subtracting cantilever deflection d with z piezo displacement Z:

$$\delta = Z - d \tag{1}$$

as illustrated in Figure 2. It is noteworthy to mention that the tip-sample contact point has to be determined before the calculation, as the z piezo has already traveled some distance before reaching the sample surface, and the previous displacement before tip-sample contact has to be excluded in order to calculate indention depth. The tip-sample contact point is marked by the onset of cantilever deflection, which is small from the beginning. As a result, the tip-sample contact point has to be estimated from the whole deflection-displacement curve.

The second step is to determine the relationship between cantilever deflection and force, which requires the calibration of cantilever sensitivity and spring constant. Cantilever sensitivity defines the relationship between cantilever deflection and detector voltage change. It is determined by pressing the tip on a hard surface, whose deformation is negligible during the measurement. By recording the z displacement ΔZ and detector voltage change ΔV, the sensitivity is given by:

$$S = \frac{\Delta V}{\Delta Z} \tag{2}$$

As the surface is assumed to be intact, the z displacement equals to the cantilever deflection. Thus in further measurements, cantilever deflection is calculated as:
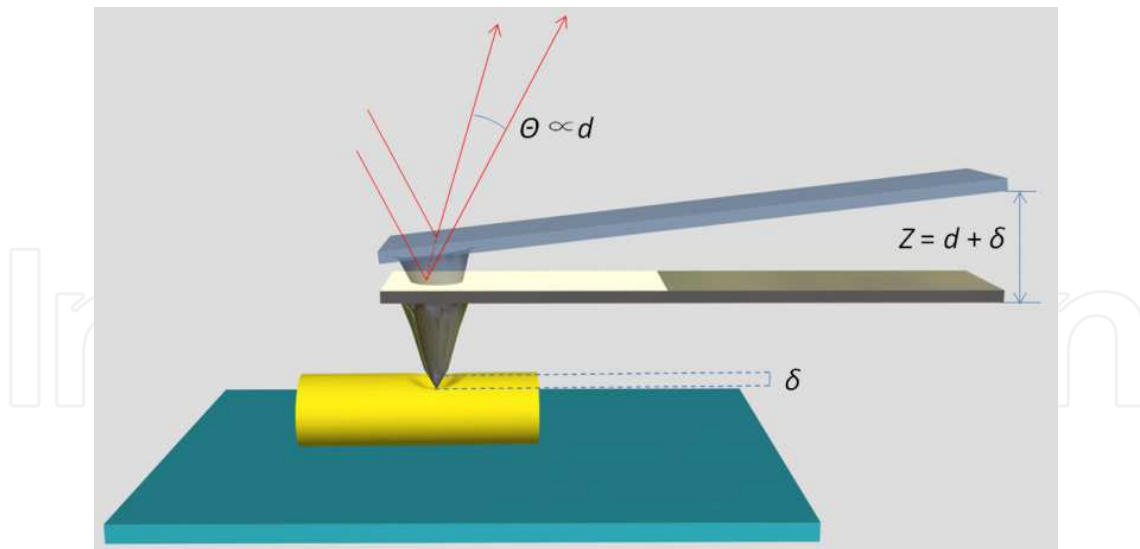
Fig. 2. The relationship of z piezo displacement (*Z*), cantilever deflection (*d*) and indentation (*δ*).

$$d = \frac{\Delta V}{S} \qquad (3)$$

A cantilever is regarded as a spring, which means the force on the tip is determined by the deflection and cantilever spring constant according to Hooke's law:

$$F = k \times d \qquad (4)$$

Every batch of AFM probe comes with a nominal value of cantilever spring constant. However, due to the systematic error generated during probe fabrication, cantilever properties vary among one batch. Therefore, it is necessary to calibrate the spring constant for each probe used. There are several methods to determine the spring constant of the cantilever with similar uncertainties (Cook, et al., 2006; Gibson et al., 2005; Ohler, 2007). The most commonly used calibration method is the thermal noise method, which has an uncertainty of 5% (Ohler, 2007).

After obtaining the force vs. indentation curve, the curve is submitted to mechanical modeling. Hertz model is a classic model of contact mechanics, which deals with two perfect elastic, homogeneous, and smooth objects pressing against each other (Johnson, 1985). The Hertzian model does not consider adhesion between the two surfaces. If adhesion forces are significant and cannot be omitted, non-Hertzian models such as the Johnson-Kendall-Roberts (JKR) model (Johnson et al., 1971) and the Derjaguin-Muller-Toporov (DMT) model (Derjaguin et al., 1975; Muller et al., 1983) should be used. The JKR and DMT model assumes the presence of short-range adhesion forces within the contact area and long-range adhesion forces outside the contact area, respectively. In most cases of amyloid indentation study, there is only insignificant adhesion between tip and sample, so the Hertz model is mainly used.

In a typical Hertz model, the AFM tip is modeled as having a paraboloidal shape. This is valid when the indentation is small compared to the tip radius, resulting in a sphere-on-flat model. If the indentation is much larger than the tip radius, then the tip can be considered as

a rigid cone, resulting in a cone-on-flat model. The latter model is called Sneddon model (Sneddon, 1965), which is a variation of Hertz model. Considering the typical indentation available in amyloid fibrils (usually less than 5 nm) and much larger tip radius (10 – 30 nm), classic Hertz model is mainly applied, which uses a paraboloidal tip shape. In this case, if the AFM tip is approximated by a sphere with the radius R, the force on the cantilever is given by:

$$F = \frac{4\sqrt{R}}{3} E^* \delta^{3/2} \tag{5}$$

where δ is the indentation depth, and E^* is the effective modulus of the tip-sample system. E^* is calculated from the following equation:

$$\frac{1}{E^*} = \frac{1 - v_{tip}^2}{E_{tip}} + \frac{1 - v_{sample}^2}{E_{sample}} \tag{6}$$

where E_{tip} , v_{tip} and E_{sample} , v_{sample} are the Young's moduli and the Poisson's ratios for the tip and sample, respectively. Usually the AFM tip is much harder than the sample, so the effective modulus is given by:

$$E^* = \frac{E_{sample}}{1 - v_{sample}^2} \tag{7}$$

Therefore the force on the cantilever is calculated as:

$$F = \frac{4E\sqrt{R}}{3\left(1 - v^2\right)} \delta^{3/2} \tag{8}$$

where E, v , R, δ . refer to the Young's modulus, Poisson's ratio, tip radius, indention depth, respectively. Poisson's ratio for amyloid is often guessed to be around 0.3.

The tip radius can be determined by two different methods. The preferred method is using electron microscopy to image the tip after the measurements (Guo & Akhremitchev, 2006). The resulting image might have a low contrast due to the low electron density of silicon nitride, which can be improved by sputtering a layer of metal on the tip. An alternative method is using the tip to scan a test sample with sharp morphology (sharper than the tip), and the resulting image can be analyzed by convolution models to get the estimated tip radius (Zenhausern et al., 1992). Previous study showed that the systematic error for the tip sample convolution method is about 30% (VanLandingham et al., 2005), which means that electron microscopy is, in principal, a more precise method to determine the tip radius. However, electron microscopy requires considerable time and effort to obtain quantifiable results.

Another concern is the finite sample thickness. When the indention depth is significant compared to the sample thickness, the sample cannot be regarded as infinitely thick. In this situation, the substrate also contributes to the mechanical response of the tip-sample system, resulting in a deviated Young's modulus. This effect can be corrected by calculating

correction factors using the uncorrected Young's modulus and normalized force (Akhremitchev & Walker, 1999; Guo & Akhremitchev, 2006). After all the calibration and approximation, the force can be linearly fitted against indentation by equation 8 and the Young's modulus is obtained.

2.2 Applications

An early AFM indentation measurement was conducted on insulin amyloid fibrils adsorbed on mica surface (Guo & Akhremitchev, 2006). The obtained force curves showed no adhesion between the tip and fibril, by which it was rationalized that the Hertz model could be used to fit the force curve. Besides, no significant indentation hysteresis was observed, suggesting a purely elastic response of the fibril to the compressive load. Considering that some fibrils were thin compared to indentation depth (height distribution ranges from 2.5 to 14 nm), correction for finite sample thickness was conducted. Variation of modulus values along the same fibril is low, suggesting similar supramolecular structure along the fibril. However, the modulus distribution among different fibrils is pretty broad, ranging from 10 to 30 MPa. The broad distribution of the Young's modulus among fibrils suggests variation in the internal packing density, and therefore different supramolecular structures (Guo & Akhremitchev, 2006), confirming the structure heterogeneity of amyloid fibrils. The result also agrees well with the observed broad distribution of the morphology, with fibril heights range from 2.5 to 14 nm. The measured Young's modulus value is significantly lower than that of the globular protein crystals (from 200 MPa to 1 GPa) (Alonso & Goldmann, 2003; Morozov & Morozova, 1993), which suggests that amyloid fibrils are relatively loosely packed, as the protofilaments are usually separated by water (Perutz et al., 2002).

It is important to note that the above method only measures the mechanical response of amyloid fibrils perpendicular to the fibril axis. It is not surprising that measured Young's modulus is low, as the fibrils are packed from protofilaments by non-specific intermolecular interactions, resulting in loose packing. However, along the fibril axis, the fibrils are constructed by β strands stacking together by intermolecular multivalent hydrogen-bonding. Thus a much higher stiffness is expected along the axis direction.

The measurement of the elastic and shear moduli along the axis are enabled by miniaturization of the standard three-point bending test with AFM (Kis et al., 2002; Salvetat et al., 1999), as illustrated in Figure 3 (Dobson, et al., 2006). Insulin amyloid fibrils are suspended over a microfabricated groove. The AFM tip was pressed against the fibril until it broke and the tip touched the bottom of the groove. The recorded force curve can be divided into four regions: region 1, the tip didn't touch the fibril; region 2, linear region, the tip contacted and deformed the fibril; region 3, nonlinear region, the tip continued to deform the fibril until it broke; region 4, linear region, the tip was pressed against the substrate, so the mechanical response corresponds to the cantilever spring constant. By considering a simple geometric model, the rupture strength of the amyloid fibril was determined to be 0.6 ± 0.4 GPa, comparable to that of spider silk (1-1.5 GPa) (Vollrath & Knight, 2001) and steel (0.6-1.8 GPa) (Shackelford et al., 1995). By measuring the mechanical response along the fibril at different fraction of the total suspended length, the results were fitted to a model and the elastic and shear moduli were determined to be $E = 3.3 \pm 0.4$ GPa and $G = 0.28 \pm 0.2$ GPa. This result confirms the previous argument that the stiffness amyloid fibril along the axis is much higher than that perpendicular to the axis.
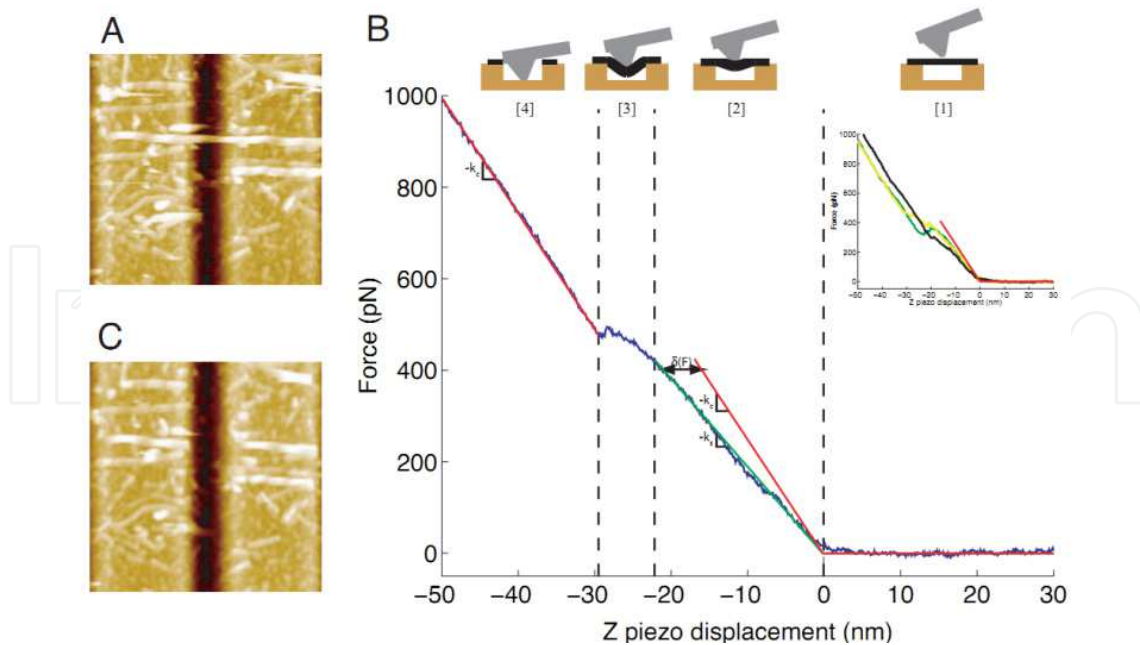
Fig. 3. Three-point bending test of amyloid fibrils with AFM (Dobson et al., 2006).

In the same paper, the authors invented a novel way to estimate the bending rigidity of the amyloid fibril. Fibrils were deposited onto mica surface, and their topographic data were acquired by tapping mode AFM and then submitted to statistical analysis based on thermal fluctuation. The resulting persistence length and bending rigidity agrees pretty well with those from force spectroscopy.

The huge difference between the axial and radial moduli is confirmed by analysis of the comparison of nanoindentation results on different location along the poly (ValGlyGlyLeuGly) amyloid fibrils (Flamia et al., 2008). As shown in Figure 4, AFM indentation was performed on three kinds of locations: fibril on silicon substrate, fibril on another fibril, and fibril suspended between two fibrils. The result is that the force versus distance curves showed identical mechanical response on different points. This result indicates that the fibril buckles instead of bends (pattern c versus pattern b in Figure 4 down part), which is the consequence of much higher axial stiffness compared to radial stiffness.
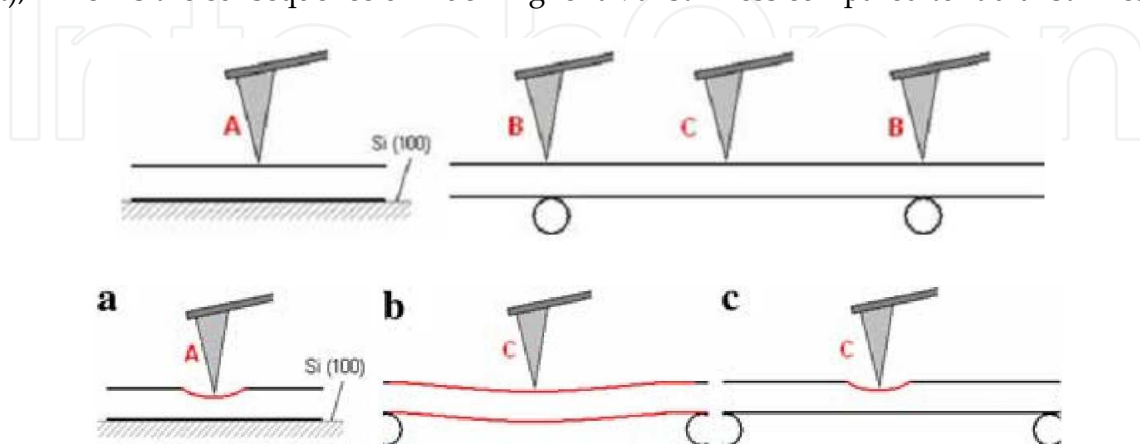

Fig. 4. Illustration of the different indentation locations along amyloid fibrils (up) and the expected deformation patterns (down) (Flamia, et al., 2008).

AFM based nanoindentation has also been applied to measure the stiffness of artificially self-assembled peptide nanotubes (Kol et al., 2005). A linear response was observed when the peptide nanotube on mica surface was pressed with AFM tip. The apparent point stiffness was obtained as the effective spring constant. The effective spring constant is the sum of the cantilever and nanotube spring constants, which gives the following relationship:

$$\frac{1}{k_{eff}} = \frac{1}{k_{cant}} + \frac{1}{k_{nano}}$$ (9)

By fitting the spring constant and the geometric configuration of the nanotube with a mechanical model, it was estimated that the Young's modulus reaches as high as 19 GPa, much higher than most biological structures such as microtubules (about 1 GPa) (de Pablo et al., 2003). The implication of the result is that artificial peptide nanotubes are even more efficiently packed than amyloid fibrils, making them promising for novel nanostructured materials.

3. AFM based force spectroscopy

3.1 General principle

The operation process of AFM based force spectroscopy is similar to that of indentation, but the purpose is quite different. A typical force spectroscopy cycle composes of four steps: (1) tip approaches the sample by vertical movement; (2) tip touches the sample with desired force and time and begins to retract; (3) tip adsorbs a molecule and stretches the molecule while retracting; (4) The molecule detaches from the surface. During the process, z piezo displacement is recorded. The extension of the molecule is calculated by subtracting cantilever deflection from z piezo displacement and adjusted according to how long the piezo has travelled before reaching the sample (maximum tip-sample separation). The resulted curve is usually called force-extension curve in force spectroscopy.

The mechanical response when a polymer molecule is stretched can be fitted by theoretical models (dash line in Figure 5 (4)). The most commonly used models are freely-jointed chain (FJC) and worm-like chain (WLC) models. Freely-jointed chain is the simplest ideal model for polymer. It assumes the polymer is composed of freely jointed rigid rods which move independently from each other. In contrast, WLC model describes the polymer chain as an isotropic, continuously flexible chain. WLC model is more suitable for stiffer polymers, with constrains between the movements of adjacent segments. As amyloid fibrils have high bending rigidity, they are modeled with WLC theory in nearly all related publications. The equation for WLC model is given as:

$$\frac{1}{\gamma} = \frac{1}{k_c \upsilon}\left(1 + \frac{k_c L_c}{4}\sqrt{\frac{F_p}{F^3}}\right)$$ (10)

Where k_c is the spring constant, υ is tip velocity, L_c and L_p are two parameters obtained from the WLC fitting, representing contour length and persistence length, respectively, F is rupture force (pN), γ is the loading rate, and
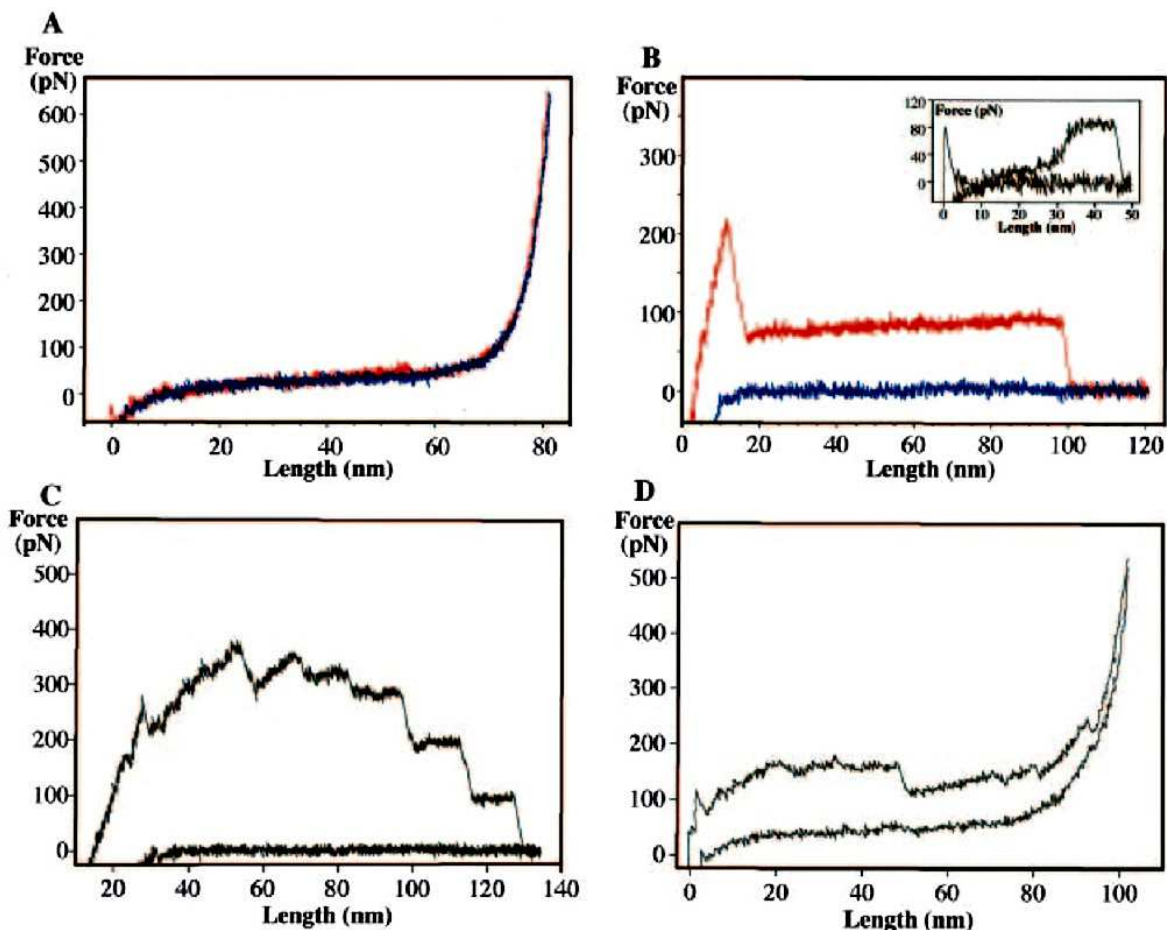
Fig. 6. Force curves of Aβ amyloid fibrils manipulated by AFM (Kellermayer, et al., 2005).

Once the force curve pattern has been recognized and related with specific interactions within the amyloid fibrils, quantitative information of the interactions can be revealed, thanks to the high sensitivity of AFM force measurement. In a following work, the unzipping force of β-sheets from the Aβ1-42 (full-length neurotoxic peptide associated with Alzheimer's disease) amyloid fibrils is compared with that of Aβ1-40 mentioned above. With two extra amino acid residues added to the C-terminus, the unzipping force falls from about 33 pN to about 23 pN, which suggests that the amyloid fibrils are destabilized by the additional two residues.

In principle, if the tip contacts the β-sheets on the amyloid fibril in the right place, a single molecular stretch should be observed. This was achieved in the AFM manipulation of amyloid fibrils formed from an 11 amino acid peptide segments of transthyratin, TTR (Fukuma et al., 2006; Mostaert & Jarvis, 2007). When the force spectroscopy was conducted on TTR fibrils, similar plateaus were observed, corresponding to the peeling off of β-sheets from the fibrils; in addition, force curves with sawtooth pattern were also captured (Figure 7), which were attributed to the successive unraveling of the peptide molecules from the fibril bulk.

The sawtooth pattern of the force spectroscopy of amyloid structures has helped identify amyloid fibrils as functional components in natural adhesive (Mostaert et al., 2006). Extracellular polymeric substances (EPS) are responsible for the adhesive properties of algae. The presence of amyloid structures were revealed by the characteristic green-gold
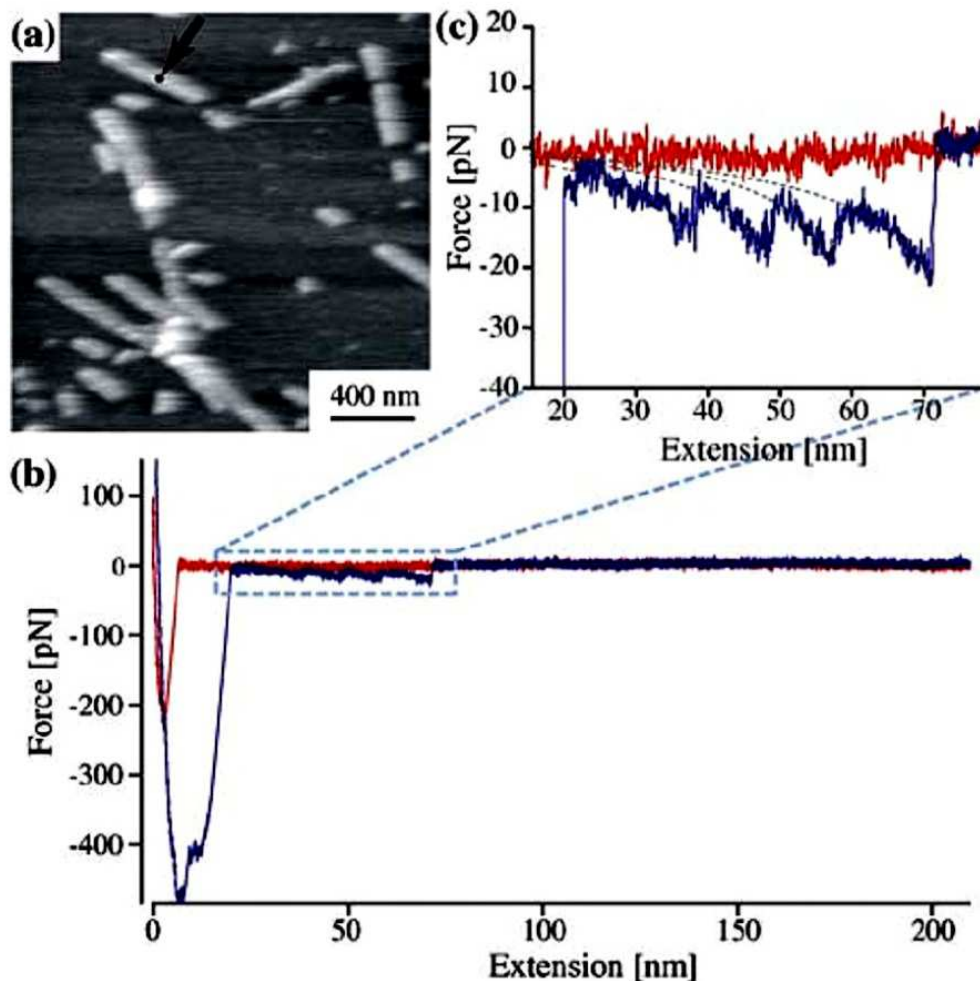
Fig. 7. Sawtooth like force curve obtained by the AFM manipulation of TTR amyloid fibrils (Fukuma, et al., 2006).

birefringence observed with cross-polarized light after Congo red dye staining. However, either direct imaging by AFM or separation from the EPS matrix is very difficult because of the complex structure and composition of EPS. However, under AFM force spectroscopy, uniform and reproducible sawtooth patterns were observed in high abundance, appearing in 20% to 50% of all the obtained force curves, depending on different regions. By fitting with WLC model, a mean persistence length of 0.34 ± 0.18 nm was obtained, which is similar to that of the titin protein (0.4 nm) (Rief, et al., 1997; Tskhovrebova, et al., 1997) or tenascin (0.42 nm) (Oberhauser et al., 1998). The mean value of the force peaks was also found to be typical for systems containing hydrogen-bonded β-sheets (Brockwell et al., 2005). Therefore, it is reasonable to propose the possible presence of highly ordered amyloid structures in EPS.

More recently, the role of amyloid fibrils in natural adhesives was confirmed by an extensive study on barnacle cement (Sullan, et al., 2009). The versatility of the AFM technique was well illustrated in this work. First, an AFM imaging was conducted to reveal the diverse morphologies of the sample, as shown in Figure 8. Then, AFM indentation tests were performed at three points in images C, D, and E. The corresponding structures were large regular rods, unstructured aggregates, and the matrix, having elastic moduli of 20-90 MPa, 0.2-2 MPa, and 1-10 MPa, respectively. Furthermore, force spectroscopy was
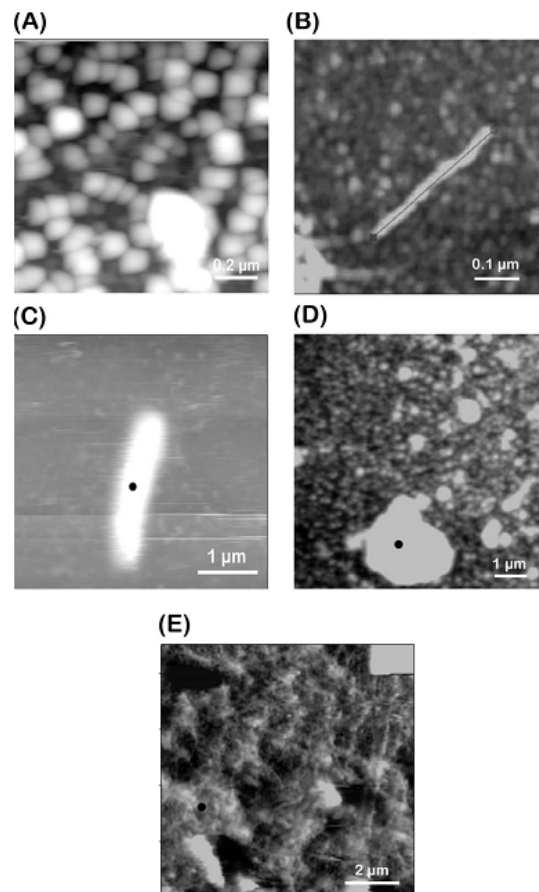
Fig. 8. A-E: Different morphologies in the barnacle cement sample. Black dots in C, D, E indicates the AFM indentation points (Sullan et al., 2009).

performed. The sawtooth pattern was observed when the tip was indented into the matrix and pulled out. However, even more periodic sawtooth pattern was obtained when the "fly-fishing" method (Rief, et al., 1997) was used. This method avoids indentation into the matrix, thus reduces the possibility of picking up multiple molecules in a single pull. Fitting the force curve with WLC model gave a persistence length of 0.35 ± 0.05 nm, which agrees pretty well with previous results on amyloid fibrils (Kellermayer, et al., 2005; Mostaert, et al., 2006). In addition, FT-IR spectroscopy and dye (Congo red and thioflavin T) staining confirmed the presence of β-sheet and amyloid structures in the sample.

The force curve patterns of amyloid fibrils under AFM manipulation are closely related to the structure and mechanical stability of the fibrils. AFM force spectroscopy on mature amyloid fibrils formed by glucagon peptides, which has uniform twisted fibrillar structures, revealed a simple force curve pattern (M. D. Dong, et al., 2008). All of the force curves exhibited non-linear elastic mechanical response followed by one or several rupture events. The absence of force plateau, which is a characteristic pattern of the unzipping of β-sheets from the fibril, implies that the high packing density in mature glucagon amyloid fibrils allows a stable confinement of the peptide molecules in the twisted fibrillar structure, in contrast to Aβ amyloid fibrils (Karsai et al., 2006; Kellermayer, et al., 2005). The stable structure is further confirmed by repeatedly stretching a single fibril for 1000 times. The resultant force curves showed surprisingly

reversible and reproducible non-linear elasticity, with a narrow distribution of both the rupture length and rupture force (Figure 9 (a)). The remarkable clean and well-defined force curves are explained by the binding of the tip to a single amyloid fibril and subsequent successive stretching between the tip and substrate, with each stretch ending with the fibril being detached from the substrate (Figure 9 (b), vi2).
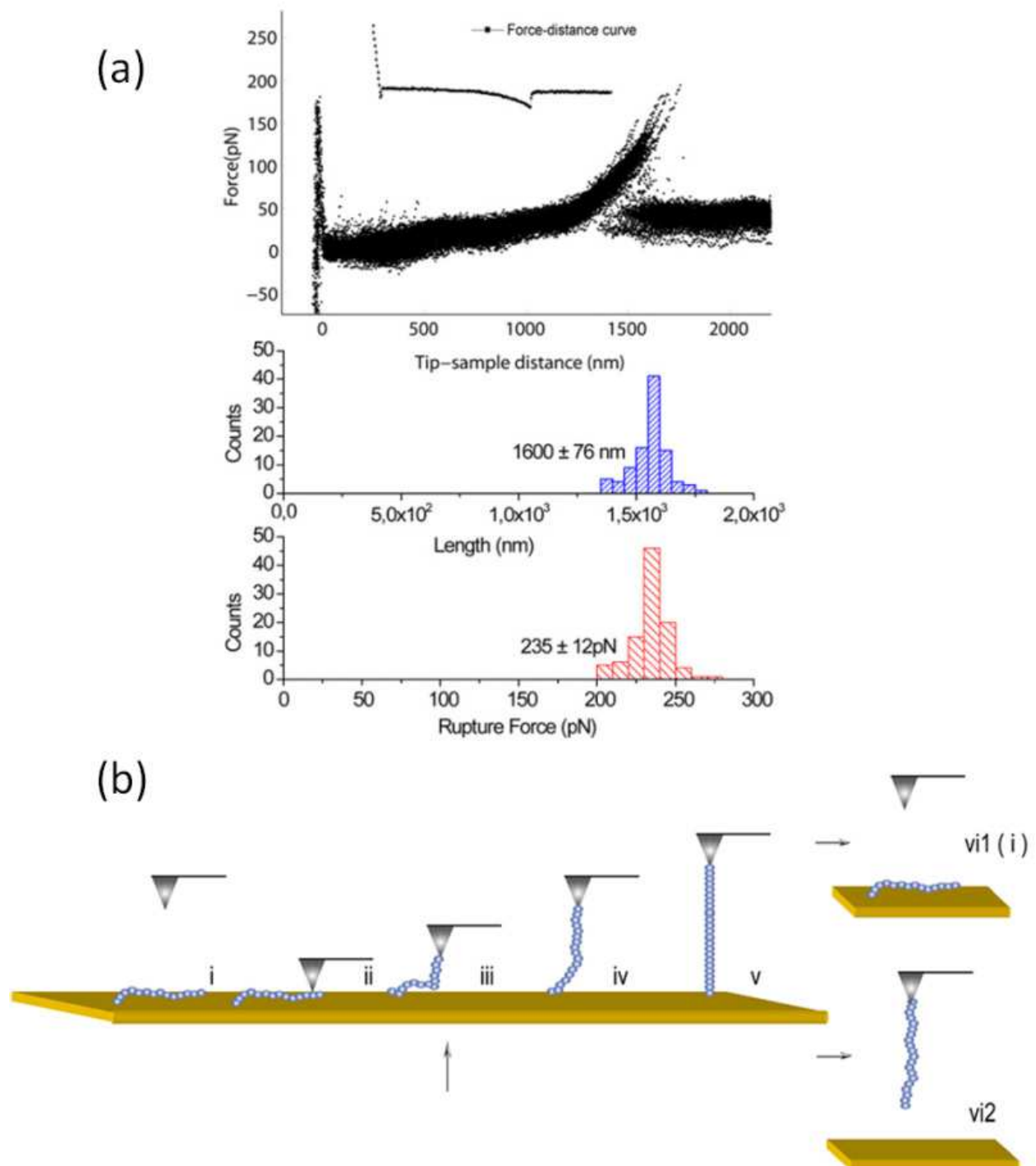

Fig. 9. Nonlinear elastic response recorded in a successive stretching (a) and schematic illustration of the possible stretching models (b) (M. D. Dong et al., 2008).

By varying the preparation conditions, the effect of disturbing factors on the mechanical stability of amyloid fibril formation can be explored. Recently, the effect of shear on the formation of β-lactoglobulin (β-Lg) amyloid fibrils is investigated with AFM imaging and force spectroscopy (Dunstan et al., 2009). Three conditions were investigated: nature environment, variable shear, and controlled shear. Force plateau, which was attributed to the peeling off of β-sheets from the amyloid fibrils, was used as an indicator of the mechanical strength of the assembled fibrils. Amyloid fibrils formed from controlled shear have significantly lower mechanical strength (force magnitude ∼20 pN) than those formed from variable shear (∼100 pN). This result indicates that variant shear induced fibrils are densely packed and well-ordered. The conclusion is further supported by AFM imaging. For variable shear induced fibrils, twisted morphology, which is of higher order, was observed. The presence of thick fibrils (5∼8 nm) was the result of the assembly of protofibrils. In contrast, the controlled shear induced fibrils have lower height (∼4 nm) and "string-of-beads" morphology, which is believed to be formed from partially unfolded monomers. Therefore, the variable shear induced fibrils are in a more mature state and those formed from controlled shear are less mature.

In most AFM based force spectroscopy measurements, the sample is attached to the tip by non-specific, intermolecular interactions. The method is straightforward and easy to perform. However, if more precise binding of the molecule is required, covalent bonding provide much more control on the binding position as well as guaranteed binding stability. In a force spectroscopy study of amyloid formed from human prion protein (PrP90-231), protein was attached by linking the engineered Cys residue to gold-covered AFM tip by gold-thiol bonding (Ganchev et al., 2008). In contrast to the irregular and poorly reproducible curves observed for the wild-type protein or Cys-variant (at position 103) probed with silicon nitride tip, similar elastic stretching was observed for each force curve of the covalently linked system. The contour length histogram from the WLC modeling of the force curves is well-defined, with 24-25 nm as the maximum, suggesting that ∼63-66 residues can be stretched entropically before the whole protein is fully pulled out from the amyloid fibrils (assuming 0.38 nm per residue in a fully extended conformation), as illustrated in Figure 10. It is reasonable to assume that the ∼63-66 residues are located out of the hydrogen-bonded core and the residues involved in the fibril core start at residue ∼166-169. Further evidence was provided by moving the engineered Cys residue to position 90, which resulted similar starting point at residue ∼164-166. Thus the results are reliable and provide important information for the structure of PrP amyloid fibrils.
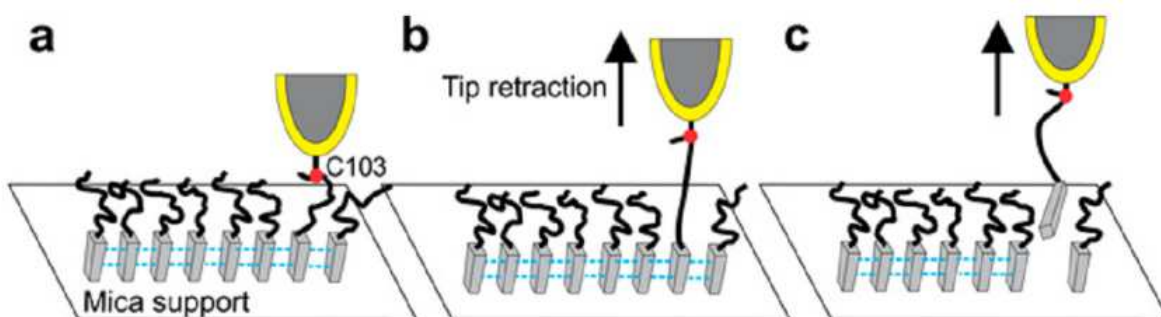

Fig. 10. Illustration of the stretching of a protein and final pull out from the core of amyloid fibrils (Ganchev, et al., 2008).

In another recent example, α-synuclein proteins (which forms amyloid associated with Parkinson's disease) were covalently attached to the tip and substrate surface separately, and their interaction was probed by AFM force spectroscopy. The testing pH was varied to investigate pH dependency. It has long been recognized that amyloid fibril formation is facilitated in acidic pH (Stine et al., 2003). The rupture force between the two proteins increases with decreasing pH, suggesting that lower pH increases the protein intermolecular interactions, facilitating protein aggregation to form amyloid fibrils, which is consistent with previous results (Lyubchenko et al., 2005). By pulling the molecules at different pulling rates, the dynamics of protein interactions can be revealed. The so-called dynamic force spectroscopy was again performed at different pH. At all pH, the rupture force increases dramatically with loading rate (pulling rate), which is defined as high loading rate dependency. By fitting with appropriate model, the lifetime of the molecular complex (dimer) was determined to be seconds, which is significantly longer than nanosecond lifetime from a recent report on structure dynamics of the α-synuclein monomer (Tsigelny et al., 2007). As a result, the formation of protein dimer significantly increases the stability of the protein molecules, which might serve as a critical nucleation step towards the aggregation of proteins to form amyloid fibrils.

4. Conclusion and perspectives

In this chapter, we have learnt from works published in the past 6 years that AFM is a powerful tool for studying the nanomechanics of amyloid materials. Typical working modes such as nanoindentation, force spectroscopy with stretching of the amyloid fibrils, or unzipping of β-sheets from the fibrils can be performed on a single platform (Figure 11 (a), (b), (c)). Combined with AFM imaging, AFM based nanoindentation makes it possible to identify a specific amyloid fibril and measure its mechanical response. The method has also revealed the huge different between the axial and radial Young's moduli of the amyloid fibrils, which is closely related to their molecular structures. AFM based force spectroscopy has showed several response pattern of amyloid fibrils under AFM manipulation. Depending on their composition and structural stability, unzipping of β-sheets, stretching of peptide molecules, stretching of an amyloid fibril have been observed. The force curve patterns, either non-linear elastic response or plateau or the superposing of the two, have been related to the morphology, packing density, stage of maturation, as well as the interactions with the environment.

The field of amyloid nanomechanics is still quite young, and what has been done has only utilized a fraction of the powerfulness of AFM. For example, covalent attachment of amyloid fibrils on the AFM tip for force spectroscopy, which will provide high accuracy and efficiency of binding, has rarely been used (Ganchev, et al., 2008; Yu et al., 2008). We expect more sophisticated AFM technique like tip modification, dynamic force spectroscopy, etc., would push AFM based research on amyloid mechanical properties to more fundamental level, single molecule force spectroscopy (SMFS), for example (Figure 11 (d)). If the tip is modified with a peptide chain or protein molecule, the interaction between single peptide or protein molecule and amyloid fibril can be probed by AFM based SMFS. The proposed method would help to identify amyloid proteins interacting with important cell surface receptors, as these proteins may be directly involved in toxicity. In addition we expect this method will also reveal more information about the surface properties, chemical composition of amyloid materials, and modulating the activity between amyloid proteins and cells.
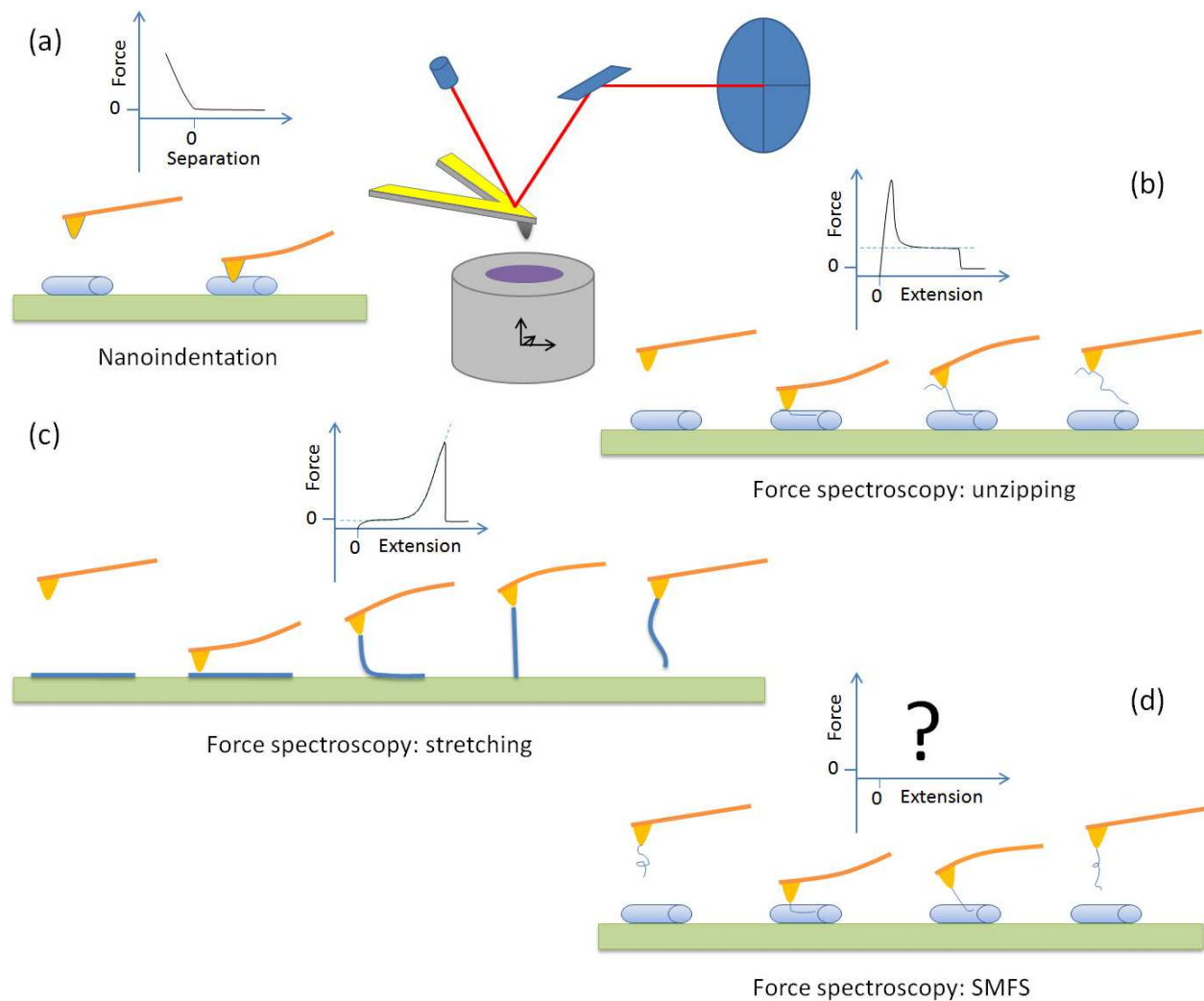
Fig. 11. Summary of AFM based study on the nanomechanics of amyloid materials and future possibility.

On the other hand, AFM is a fast-developing technique, with new progresses being made every year. Among them, quantitative nanomechanical mapping (QNM) (M. Dong & Sahin, 2011; M. D. Dong et al., 2009) is noteworthy, as it has already been applied to measurement mechanical properties of amyloid fibrils (Adamcik et al., 2011; Sweers et al., 2011). QNM records a force curve at every point on the sample and uses peak force value of the force curve as imaging feedback. The advantage is that mechanical properties such as Young's modulus, adhesion, deformation, and dissipation can be calculated and exported simultaneously in real time. QNM makes the measurement of surface mechanical properties quite straightforward (Adamcik, et al., 2011).

The ability of mapping surface mechanical properties without compromising the resolution is attractive, as it will be helpful to study the heterogeneity of amyloid fibrils, identifying different stages of amyloid growth.

However, potential problems may exist in the convenient measurement technique. Because normally data analysis is automatically processed, users have limited control, which makes

it hard to correct errors from finite sample thickness, deviation from standard model, etc., according to the specific system investigated (Sweers, et al., 2011). Thus it is still very important to understand the data analysis process and evaluate potential system errors it may bring about.

5. References

Adamcik, J., Berquand, A., & Mezzenga, R. (2011). Single-step direct measurement of amyloid fibrils stiffness by peak force quantitative nanomechanical atomic force microscopy. *Applied Physics Letters, 98* (19), 193701.

Akhremitchev, B. B., & Walker, G. C. (1999). Finite sample thickness effects on elasticity determination using atomic force microscopy. *Langmuir, 15* (17), 5630-5634.

Alonso, J. L., & Goldmann, W. H. (2003). Feeling the forces: atomic force microscopy in cell biology. *Life Sciences, 72* (23), 2553-2560.

Ashkin, A., Dziedzic, J. M., Bjorkholm, J. E., & Chu, S. (1986). Observation of a Single-Beam Gradient Force Optical Trap for Dielectric Particles. *Optics Letters, 11* (5), 288-290.

Barrau, S., Zhang, F., Herland, A., Mammo, W., Andersson, M. R., & Inganas, O. (2008). Integration of amyloid nanowires in organic solar cells. *Applied Physics Letters, 93* (2), 023307.

Binnig, G., Quate, C. F., & Gerber, C. (1986). Atomic Force Microscope. *Physical Review Letters, 56* (9), 930-933.

Brockwell, D. J., Beddard, G. S., Paci, E., West, D. K., Olmsted, P. D., Smith, D. A., et al. (2005). Mechanically unfolding the small, topologically simple protein L. *Biophysical Journal, 89* (1), 506-519.

Bucciantini, M., Giannoni, E., Chiti, F., Baroni, F., Formigli, L., Zurdo, J. S., et al. (2002). Inherent toxicity of aggregates implies a common mechanism for protein misfolding diseases. *Nature, 416* (6880), 507-511.

Carny, O., Shalev, D. E., & Gazit, E. (2006). Fabrication of coaxial metal nanocables using a self-assembled peptide nanotube scaffold. *Nano Letters, 6* (8), 1594-1597.

Channon, K. J., Devlin, G. L., & MacPhee, C. E. (2009). Efficient Energy Transfer within Self-Assembling Peptide Fibers: A Route to Light-Harvesting Nanomaterials. *Journal of the American Chemical Society, 131* (35), 12520-12521.

Chapman, M. R., Robinson, L. S., Pinkner, J. S., Roth, R., Heuser, J., Hammar, M., et al. (2002). Role of Escherichia coli curli operons in directing amyloid fiber formation. *Science, 295* (5556), 851-855.

Chiti, F., & Dobson, C. M. (2006). Protein misfolding, functional amyloid, and human disease. *Annual Review of Biochemistry, 75*, 333-366.

Cook, S., Schaffer, T. E., Chynoweth, K. M., Wigton, M., Simmonds, R. W., & Lang, K. M. (2006). Practical implementation of dynamic methods for measuring atomic force microscope cantilever spring constants. *Nanotechnology, 17* (9), 2135-2145.

de Pablo, P. J., Schaap, I. A. T., MacKintosh, F. C., & Schmidt, C. F. (2003). Deformation and collapse of microtubules on the nanometer scale. *Physical Review Letters, 91* (9), 098101.

Derjaguin, B. V., Muller, V. M., & Toporov, Y. P. (1975). Effect of contact deformations on the adhesion of particles. *Journal of Colloid and Interface Science, 53* (2), 314-326.

Dobson, C. M. (1999). Protein misfolding, evolution and disease. *Trends in Biochemical Sciences, 24* (9), 329-332.

Dobson, C. M., Smith, J. F., Knowles, T. P. J., MacPhee, C. E., & Welland, M. E. (2006). Characterization of the nanoscale properties of individual amyloid fibrils. *Proceedings of the National Academy of Sciences of the United States of America, 103* (43), 15806-15811.

Dong, M., & Sahin, O. (2011). A nanomechanical interface to rapid single-molecule interactions. [10.1038/ncomms1246]. *Nature Communications, 2*, 247.

Dong, M. D., Hovgaard, M. B., Mamdouh, W., Xu, S. L., Otzen, D. E., & Besenbacher, F. (2008). AFM-based force spectroscopy measurements of mature amyloid fibrils of the peptide glucagon. *Nanotechnology, 19* (38), 384013.

Dong, M. D., Husale, S., & Sahin, O. (2009). Determination of protein structural flexibility by microsecond force spectroscopy. *Nature Nanotechnology, 4* (8), 514-517.

Dunstan, D. E., Hamilton-Brown, P., Asimakis, P., Ducker, W., & Bertolini, J. (2009). Shear-induced structure and mechanics of beta-lactoglobulin amyloid fibrils. *Soft Matter, 5* (24), 5020-5028.

Ellis-Behnke, R. G., Liang, Y. X., You, S. W., Tay, D. K. C., Zhang, S. G., So, K. F., et al. (2006). Nano neuro knitting: Peptide nanofiber scaffold for brain repair and axon regeneration with functional return of vision (vol 103, pg 5054, 2006). *Proceedings of the National Academy of Sciences of the United States of America, 103* (19), 7530-7530.

Flamia, R., Zhdan, P. A., Castle, J. E., & Tamburro, A. M. (2008). Comment on the mechanical properties of the amyloid fibre, poly (ValGlyGlyLeuGly), obtained by a novel AFM methodology. *Journal of Materials Science, 43* (1), 395-397.

Fowler, D. M., Koulov, A. V., Alory-Jost, C., Marks, M. S., Balch, W. E., & Kelly, J. W. (2005). Functional Amyloid Formation within Mammalian Tissue. *PLoS Biol, 4* (1), e6.

Fowler, D. M., Koulov, A. V., Balch, W. E., & Kelly, J. W. (2007). Functional amyloid – from bacteria to humans. *Trends in Biochemical Sciences, 32* (5), 217-224.

Fukuma, T., Mostaert, A. S., & Jarvis, S. P. (2006). Explanation for the mechanical strength of amyloid fibrils. *Tribology Letters, 22* (3), 233-237.

Ganchev, D. N., Cobb, N. J., Surewicz, K., & Surewicz, W. K. (2008). Nanomechanical properties of human prion protein amyloid as probed by force spectroscopy. *Biophysical Journal, 95* (6), 2909-2915.

Gibson, C. T., Smith, D. A., & Roberts, C. J. (2005). Calibration of silicon atomic force microscope cantilevers. *Nanotechnology, 16* (2), 234-238.

Guo, S., & Akhremitchev, B. B. (2006). Packing Density and Structural Heterogeneity of Insulin Amyloid Fibrils Measured by AFM Nanoindentation. *Biomacromolecules, 7* (5), 1630-1636.

Holmes, T. C., de Lacalle, S., Su, X., Liu, G. S., Rich, A., & Zhang, S. G. (2000). Extensive neurite outgrowth and active synapse formation on self-assembling peptide scaffolds. *Proceedings of the National Academy of Sciences of the United States of America, 97* (12), 6728-6733.

Jaroniec, C. P., MacPhee, C. E., Bajaj, V. S., McMahon, M. T., Dobson, C. M., & Griffin, R. G. (2004). High-resolution molecular structure of a peptide in an amyloid fibril determined by magic angle spinning NMR spectroscopy. *Proceedings of the National Academy of Sciences of the United States of America, 101* (3), 711-716.

Johnson, K. L. (1985). Contact mechanics. Cambridge, U.K.: Cambridge University Press.

Johnson, K. L., Kendall, K., & Roberts, A. D. (1971). Surface Energy and the Contact of Elastic Solids. *Proceedings of the Royal Society of London. A. Mathematical and Physical Sciences, 324* (1558), 301-313.

Karsai, Á., Mártonfalvi, Z., Nagy, A., Grama, L., Penke, B., & Kellermayer, M. S. Z. (2006). Mechanical manipulation of Alzheimer's amyloid β1–42 fibrils. *Journal of Structural Biology, 155* (2), 316-326.

Kellermayer, M. S. Z., Grama, L., Karsai, A., Nagy, A., Kahn, A., Datki, Z. L., et al. (2005). Reversible mechanical unzipping of amyloid beta-fibrils. *Journal of Biological Chemistry, 280* (9), 8464-8470.

Kis, A., Kasas, S., Babic, B., Kulik, A. J., Benoit, W., Briggs, G. A. D., et al. (2002). Nanomechanics of microtubules. *Physical Review Letters, 89* (24), 248101.

Kol, N., Adler-Abramovich, L., Barlam, D., Shneck, R. Z., Gazit, E., & Rousso, I. (2005). Self-assembled peptide nanotubes are uniquely rigid bioinspired supramolecular structures. *Nano Letters, 5* (7), 1343-1346.

Liang, Y., Guo, P., Pingali, S. V., Pabit, S., Thiyagarajan, P., Berland, K. M., et al. (2008). Light harvesting antenna on an amyloid scaffold. *Chemical Communications* (48), 6522-6524.

Luhrs, T., Ritter, C., Adrian, M., Riek-Loher, D., Bohrmann, B., Doeli, H., et al. (2005). 3D structure of Alzheimer's amyloid-beta (1-42) fibrils. *Proceedings of the National Academy of Sciences of the United States of America, 102* (48), 17342-17347.

Lyubchenko, Y. L., McAllister, C., Karymov, M. A., Kawano, Y., Lushnikov, A. Y., Mikheikin, A., et al. (2005). Protein interactions and misfolding analyzed by AFM force spectroscopy. *Journal of Molecular Biology, 354* (5), 1028-1042.

Maji, S. K., Schubert, D., Rivier, C., Lee, S., Rivier, J. E., & Riek, R. (2008). Amyloid as a depot for the formulation of long-acting drugs. *Plos Biology, 6* (2), 240-252.

Morozov, V. N., & Morozova, T. Y. (1993). Elasticity of Globular-Proteins - the Relation between Mechanics, Thermodynamics and Mobility. *Journal of Biomolecular Structure & Dynamics, 11* (3), 459-481.

Mostaert, A. S., Higgins, M. J., Fukuma, T., Rindi, F., & Jarvis, S. P. (2006). Nanoscale mechanical characterisation of amyloid fibrils discovered in a natural adhesive. *Journal of Biological Physics, 32* (5), 393-401.

Mostaert, A. S., & Jarvis, S. P. (2007). Beneficial characteristics of mechanically functional amyloid fibrils evolutionarily preserved in natural adhesives. *Nanotechnology, 18* (4).

Muller, V. M., Derjaguin, B. V., & Toporov, Y. P. (1983). On two methods of calculation of the force of sticking of an elastic sphere to a rigid plane. *Colloids and Surfaces, 7* (3), 251-259.

Neuman, K. C., & Nagy, A. (2008). Single-molecule force spectroscopy: optical tweezers, magnetic tweezers and atomic force microscopy. [10.1038/nmeth.1218]. *Nature Methods, 5* (6), 491-505.

Oberhauser, A. F., Marszalek, P. E., Erickson, H. P., & Fernandez, J. M. (1998). The molecular elasticity of the extracellular matrix protein tenascin. *Nature, 393* (6681), 181-185.

Oda, T., Wals, P., Osterburg, H. H., Johnson, S. A., Pasinetti, G. M., Morgan, T. E., et al. (1995). Clusterin (Apoj) Alters the Aggregation of Amyloid Beta-Peptide (a-Beta (1-42)) and Forms Slowly Sedimenting a-Beta Complexes That Cause Oxidative Stress. *Experimental Neurology, 136* (1), 22-31.

Ohler, B. (2007). Cantilever spring constant calibration using laser Doppler vibrometry. *Review of Scientific Instruments, 78* (6), 063701.

Paravastu, A. K., Leapman, R. D., Yau, W. M., & Tycko, R. (2008). Molecular structural basis for polymorphism in Alzheimer's beta-amyloid fibrils. *Proceedings of the National Academy of Sciences of the United States of America, 105* (47), 18349-18354.

Perutz, M. F., Finch, J. T., Berriman, J., & Lesk, A. (2002). Amyloid fibers are water-filled nanotubes. *Proceedings of the National Academy of Sciences of the United States of America, 99* (8), 5591-5595.

Reches, M., & Gazit, E. (2003). Casting metal nanowires within discrete self-assembled peptide nanotubes. *Science, 300* (5619), 625-627.

Rief, M., Gautel, M., Oesterhelt, F., Fernandez, J. M., & Gaub, H. E. (1997). Reversible unfolding of individual titin immunoglobulin domains by AFM. *Science, 276* (5315), 1109-1112.

Salvetat, J. P., Briggs, G. A. D., Bonard, J. M., Bacsa, R. R., Kulik, A. J., Stockli, T., et al. (1999). Elastic and shear moduli of single-walled carbon nanotube ropes. *Physical Review Letters, 82* (5), 944-947.

Sawaya, M. R., Sambashivan, S., Nelson, R., Ivanova, M. I., Sievers, S. A., Apostol, M. I., et al. (2007). Atomic structures of amyloid cross-beta spines reveal varied steric zippers. *Nature, 447* (7143), 453-457.

Scheibel, T., Parthasarathy, R., Sawicki, G., Lin, X. M., Jaeger, H., & Lindquist, S. L. (2003). Conducting nanowires built by controlled self-assembly of amyloid fibers and selective metal deposition. *Proceedings of the National Academy of Sciences of the United States of America, 100* (8), 4527-4532.

Selkoe, D. J. (2001). Alzheimer's disease: Genes, proteins, and therapy. *Physiological Reviews, 81* (2), 741-766.

Shackelford, J., Alexander, W., & Park, J. (1995). *CRC Practical Handbook of Materials Selection* (1st Ed ed.). Boca Raton, FL: CRC.

Shibayama, Y., Joseph, K., Nakazawa, Y., Ghebreihiwet, B., Peerschke, E. I. B., & Kaplan, A. P. (1999). Zinc-dependent activation of the plasma kinin-forming cascade by aggregated beta amyloid protein. *Clinical Immunology, 90* (1), 89-99.

Sneddon, I. N. (1965). The Relation between Load and Penetration in the Axisymmetric Boussinesq Problem for a Punch of Arbitrary Profile. *INt. J. Eng. Sci., 3*, 11.

Stine, W. B., Dahlgren, K. N., Krafft, G. A., & LaDu, M. J. (2003). In vitro characterization of conditions for amyloid-beta peptide oligomerization and fibrillogenesis. *Journal of Biological Chemistry, 278* (13), 11612-11622.

Strick, T., Allemand, J. F., Croquette, V., & Bensimon, D. (2000). Twisting and stretching single DNA molecules. *Progress in Biophysics & Molecular Biology, 74* (1-2), 115-140.

Sullan, R. M. A., Gunari, N., Tanur, A. E., Yuri, C., Dickinson, G. H., Orihuela, B., et al. (2009). Nanoscale structures and mechanics of barnacle cement. *Biofouling, 25* (3), 263-275.

Sweers, K., van der Werf, K., Bennink, M., & Subramaniam, V. (2011). Nanomechanical properties of alpha-synuclein amyloid fibrils: a comparative study by nanoindentation, harmonic force microscopy, and Peakforce QNM. *Nanoscale Research Letters, 6, 270.*

Tan, S. Y., & Pepys, M. B. (1994). Amyloidosis. *Histopathology, 25* (5), 403-414.

Toyama, B. H., & Weissman, J. S. (2011). Amyloid Structure: Conformational Diversity and Consequences. In R. D. Kornberg, C. R. H. Raetz, J. E. Rothman & J. W. Thorner (Eds.), *Annual Review of Biochemistry, Vol 80* (Vol. 80, pp. 557-585).

Tsigelny, I. F., Bar-On, P., Sharikov, Y., Crews, L., Hashimoto, M., Miller, M. A., et al. (2007). Dynamics of alpha-synuclein aggregation and inhibition of pore-like oligomer development by beta-synuclein. *Febs Journal, 274* (7), 1862-1877.

Tskhovrebova, L., Trinick, J., Sleep, J. A., & Simmons, R. M. (1997). Elasticity and unfolding of single molecules of the giant muscle protein titin. *Nature, 387* (6630), 308-312.

VanLandingham, M. R., Juliano, T. F., & Hagon, M. J. (2005). Measuring tip shape for instrumented indentation using atomic force microscopy. *Measurement Science & Technology, 16* (11), 2173-2185.

Vollrath, F., & Knight, D. P. (2001). Liquid crystalline spinning of spider silk. *Nature, 410* (6828), 541-548.

Wasmer, C., Lange, A., Van Melckebeke, H., Siemer, A. B., Riek, R., & Meier, B. H. (2008). Amyloid fibrils of the HET-s (218-289) prion form a beta solenoid with a triangular hydrophobic core. *Science, 319* (5869), 1523-1526.

Weisenhorn, A. L., Hansma, P. K., Albrecht, T. R., & Quate, C. F. (1989). Forces in Atomic Force Microscopy in Air and Water. *Applied Physics Letters, 54* (26), 2651-2653.

Westermark, G. T., Johnson, K. H., & Westermark, P. (1999). [1] Staining methods for identification of amyloid in tissue. In W. Ronald (Ed.), *Methods in Enzymology* (Vol. Volume 309, pp. 3-25): Academic Press.

Yu, J., Malkova, S., & Lyubchenko, Y. L. (2008). α-Synuclein Misfolding: Single Molecule AFM Force Spectroscopy Study. *Journal of Molecular Biology, 384* (4), 992-1001.

Zenhausern, F., Adrian, M., Tenheggelerbordier, B., Eng, L. M., & Descouts, P. (1992). DNA and Rna-Polymerase DNA Complex Imaged by Scanning Force Microscopy - Influence of Molecular-Scale Friction. *Scanning, 14* (4), 212-217.
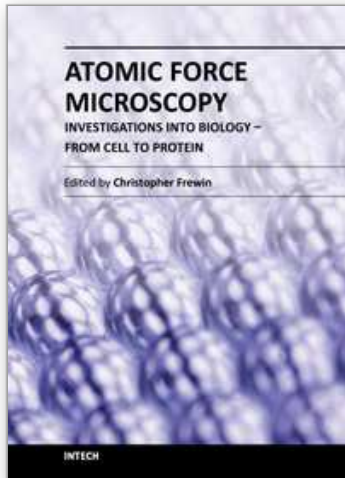
Atomic Force Microscopy Investigations into Biology - From Cell to Protein

Edited by Dr. Christopher Frewin

The atomic force microscope (AFM) has become one of the leading nanoscale measurement techniques for materials science since its creation in the 1980's, but has been gaining popularity in a seemingly unrelated field of science: biology. The AFM naturally lends itself to investigating the topological surfaces of biological objects, from whole cells to protein particulates, and can also be used to determine physical properties such as Young's modulus, stiffness, molecular bond strength, surface friction, and many more. One of the most important reasons for the rise of biological AFM is that you can measure materials within a physiologically relevant environment (i.e. liquids). This book is a collection of works beginning with an introduction to the AFM along with techniques and methods of sample preparation. Then the book displays current research covering subjects ranging from nano-particulates, proteins, DNA, viruses, cellular structures, and the characterization of living cells.

How to reference

In order to correctly reference this scholarly work, feel free to copy and paste the following:

Guanghong Zeng, Yusheng Duan, Flemming Besenbacher and Mingdong Dong (2012). Nanomechanics of Amyloid Materials Studied by Atomic Force Microscopy, Atomic Force Microscopy Investigations into Biology - From Cell to Protein, Dr. Christopher Frewin (Ed.), ISBN: 978-953-51-0114-7, InTech, Available from: http://www.intechopen.com/books/atomic-force-microscopy-investigations-into-biology-from-cell-to-protein/nanomechanical-properties-of-amyloid-proteins-studied-by-afm

INTECH
open science | open minds